ASTRONOMY AND SPACE SCIENCE
www.csiro.au

On-Dish Calibration of XY Phase for ASKAP's Phased Array Feeds

Aaron Chippendale and Craig Anderson

ASKAP Commissioning and Early Science Memo 019
April 15, 2019

CSIRO Astronomy and Space Science
Cnr Vimiera & Pembroke Roads, Marsfield, NSW 2122, Australia
PO Box 76, Epping, NSW 1710, Australia
Telephone : +61 2 9372 4100
Fax : +61 2 9372 4310

Copyright and disclaimer

Important disclaimer

Contents

1 Summary

The Australian Square Kilometre Pathfinder (ASKAP) telescope uses external noise sources to maintain calibration of its phased-array-feed (PAF) beams. We describe a new technique for estimating the XY phase of PAF beams via this same On-Dish Calibration (ODC) system. Further, we demonstrate successful adjustment of beamformer weights so that the XY phase of each dual-polarisation beam pair is near zero by design. Validation against the existing method of XY phase calibration, with one rotated ASKAP antenna, shows that our new technique yields band-average XY phase of $0.34^{+5}_{-4.4}$ degrees for 95% of PAF beams.

Our results allow polarisaiton studies to be made commensaly with all ASKAP observations. Previously, ASKAP has used beamformer weights with arbitrary XY phase. This required time-consuming interferometry measurements with the full ASKAP array to determine XY phase with the added complications of having to offset the roll axis of one antenna and apply a specialised polarisation calibration and imaging pipeline. Calibrating XY phase up-front in the beamformer weights allows polarisation calibration and imaging to take place within the standard ASKAP software pipeline.

In earlier work, Dowson (2017) explored the utility of the ODC system for PAF diagnostics and calibration and Chippendale et al. (2018) investigated the ODC signal level and its impact on beam sensitivity. ODC systems are now fully operational on all 36 ASKAP antennas and weights with XY-phase calibrated via the ODCs are now used by default.

2 Legacy XY Phase Calibration via Rotated Antenna

Until recently, beamformer weights for ASKAP PAF beams have been generated via the maximum sensitivity algorithm following the procedure described in McConnell et al. (2016). This method makes a minor correction to the otherwise arbitrary phase of the maximum sensitivity algorithm to ensure phase smoothness across frequency for each PAF beam. However this method does not constrain the phase between X and Y beams pointing in the same direction, which we call the XY phase of the PAF beam.

To date, we have calibrated XY phase via intentional misalignment of the roll axis of one ASKAP antenna by 5° (Sault, 2014). This intentional roll-axis offset is maintained during beamforming, bandpass calibration, and science observations. ASKAP beams have so far been formed in a biscalar fashion that only uses X-polarisation PAF ports to make X-polarisation beams and only Y-polarisation PAF ports to make Y-polarisation beams. Sault (2014) showed that there is low leakage between the X and Y-polarisation beams so formed. The intentional misalignment of the roll axis of one antenna by 5° introduces a $\sin 5^\circ \approx 9\%$ leakage between the X beam on the misaligned ASKAP antenna and the Y beams on all other antennas that point in the same direction. This leakage can be measured by observing an unpolarised astronomical source at the beam centre and used to derive XY phase. Solution for XY phase via the misaligned roll-axis technique on ASKAP is described by Anderson et al. (2018) and is similar to an approach previously used at Westerbork (Weiler, 1973). This strategy has lead to a non-standard software pipeline for processing polarisation information from ASKAP observations (Anderson et al., 2019 - in prep). The inclusion of a misaligned antenna in polarisation observations has also complicated processing of these observations with the standard ASKAP calibration and imaging software pipeline.

3 Why Calibrate XY Phase via External Noise Sources?

It is inconvenient to rotate the roll axis of one ASKAP antenna and invoke a special software pipeline for polarisation measurements with ASKAP. Our approach is to use external noise sources to measure the XY phase of each dual-polarisation pair of PAF beams and adjust the phase of the Y-polarisation beamformer weights so that the XY phase becomes close to zero by design. Near-zero XY phase allows polarisation to be measured in typical ASKAP observations with standard observational procedures and the standard calibration and imaging pipeline. Polarisaiton studies can then be made commensaly with all ASKAP observations.

The new XY phase calibration takes place during the initial calculation of beamformer weights and does not require additional measurements or processing effort compared to the current method used on ASKAP for maxSNR PAF beams (McConnell et al., 2016). It is merely necessary to have the external noise sources turned on during measurements already required for calculating maxSNR weights. If PAF beams are made with near-zero XY phase, it is no longer necessary to misalign the roll axis of one antenna or use the dedicated polarisation processing pipeline. The following sections describe the On-Dish Calibration System, how we use it to estimate and correct XY phase via the beamformer weights, and how we validated that the XY phase of corrected beams is near zero.

4 ASKAP's On-Dish Calibration System

ASKAP uses external noise sources to maintain calibration of PAF beams. For convenience we reproduce the following description of the system from Chippendale et al. (2018). Figure 4.1 shows a functional schematic of the on-dish calibration (ODC) system (Beresford et al., 2018) that is installed for each ASKAP antenna. Each reflector antenna has a dedicated broadband noise source collocated with its digital backend at the central site. The calibration noise is transported via radio frequency over fibre (RFoF) to a small antenna, mounted at the vertex of each paraboloidal reflector, that radiates the noise into the PAF.

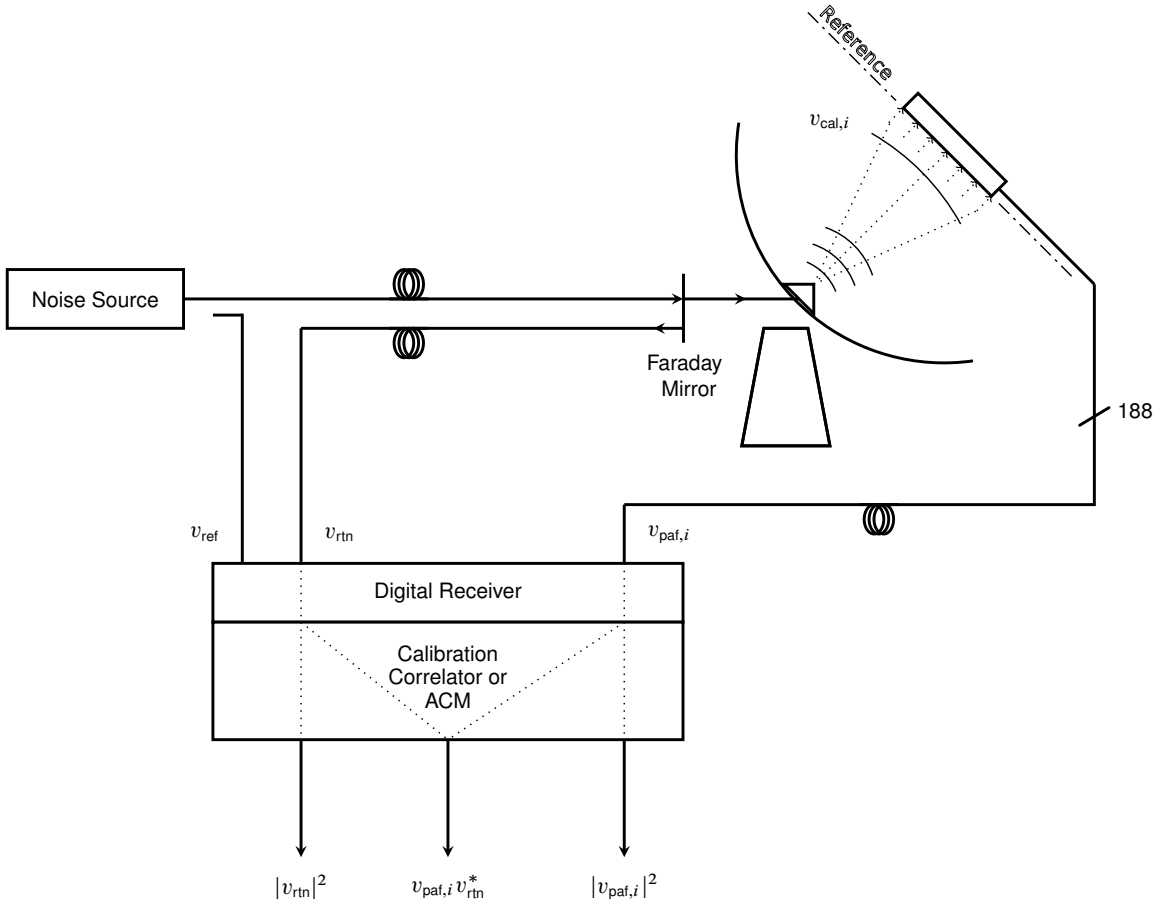

Figure 4.1: Schematic of the on-dish calibration (ODC) system (from Chippendale et al., 2018).

Near the point where the calibration signal is converted back to an electrical signal for radiation into the PAF, a portion of the optical signal is reflected back along the fibre to the digital receiver (Brown et al., 2014) at the central site. This "return" copy v_{rtn} of the calibration signal travels a similar distance back to the digital receiver as the radiated signal $v_{\mathrm{cal},i}$ received at the i^{th} PAF port. A "reference" copy v_{ref} of the calibration signal is also directly injected into the digital receiver. This may be used in the future to extract the component of calibration corrections due to the RFoF link. We used the Array Covariance Module (ACM), implemented in the firmware of ASKAP's "Redback" beamformer hardware (Hampson et al., 2014), to correlate the signals $v_{\mathrm{paf},i}$ received via each PAF port with v_{rtn}. The correlations required for calibration are in the columns of the covariance matrix corresponding to v_{ref} and v_{rtn}. All covariance matrices used for beamforming and XY phase estimation in this work used a wall-clock integration time of 2 s. Actual integration time was 0.5 s because the ACM inputs are decimated by four in firmware.

5 Measuring XY Phase via On-Dish Calibration

For each beam pointing and in each 1 MHz coarse-filterbank channel we follow the procedure of McConnell et al. (2016) to independently make beamformer weights for the two PAF polarisations: $\mathbf{w}_x$ using only the covariance between PAF ports 1 to 94 which we refer to as X polarisation ports and $\mathbf{w}_y$ using only the covariance between PAF ports 95 to 188 which we refer to as Y polarisation ports. See Reynolds (2014) for a definition of the PAF port numbering and coordinates defining the orientation of the PAF with respect to an ASKAP antenna and the sky.

We define $\mathbf{w}_x$ and $\mathbf{w}_y$ both to be 188 elements long, but $\mathbf{w}_x$ is identically zero for elements 95 to 188 and $\mathbf{w}_y$ is identically zero for elements 1 to 94. Further, when we make full-sized ASKAP beam footprints of 36 dual-polarisation beams, firmware resource limitations mean we can only support 60 non-zero weights for each single polarisation beam. Hence a further $94 - 60 = 34$ elements in each of $\mathbf{w}_x$ and $\mathbf{w}_y$ are set to zero.

In the current work we set to zero the ports with smallest weight amplitude. This is not the optimum strategy, we should actually set to zero the beamformer weights that together make the smallest joint contribution to the beamformed signal-to-noise ratio. However, selecting on weight amplitude is reasonable when all ports on a given PAF are functional, have a similar bandpass, and are set to a common operating level by adjusting RF attenuators. These conditions are typically met by ASKAP's PAFs with current operating procedures. We will discuss a more robust strategy for selecting which PAF ports to include in a given beam in a future work and proceed here using weight amplitude only. Our XY phase estimation and correction results turn out to be good despite this simplification, and should only improve as we revisit the technique with more robust port selection.

We use the technique of Chippendale et al. (2016) to disembed the PAF port gains from the beam weights $\mathbf{w}_x$ to yield idealised weights $\mathbf{w}'_x$ referred to the calibration source. In the ideal case the calibration source would present a plane wave to the PAF, illuminating every port equally and in phase. In this case, the calibrated weights of a given beam are a good estimate of the focal field exciting the PAF when the telescope observes a point source in the centre of that beam. The calibrated weights are given by the element-wise (Hadamard) product of maxSNR beamformer weights by the conjugate of an estimate of the PAF's response to a plane wave $\mathbf{s}_{\text{cal}}$ as follows

$$\mathbf{w}'_x = \mathbf{s}^*_{\text{cal}} \circ \mathbf{w}. \tag{5.1}$$

The PAF's response to a plane wave is estimated via the correlation of the voltage received at each PAF port $\mathbf{v}_{\text{paf}}$, while illuminated by the external calibration noise, with a copy of the calibration noise v_{rtn} that is returned to the digital receiver for relative gain and phase referencing of all PAF ports

$$\mathbf{s}_{\text{cal}} = \left\langle \mathbf{v}_{\text{paf}} v^*_{\text{rtn}} \right\rangle. \tag{5.2}$$

The ODC response $\mathbf{s}_{\text{cal}}$ of the PAF is measured via the column of the ACM corresponding to the correlations between each PAF port and the return copy of the calibration noise as shown in Figure 4.1. $\mathbf{w}'_x$ is then an estimate of the relative gain and phase weighting of each PAF port in a maxSNR PAF beam referred back to a near-plane wave at the PAF LNA inputs, as received from the calibration source at the vertex of the paraboloidal reflector. This is a fair estimate of the amplitude and phase of the field sampled by the PAF at the focal plane of the reflector.

The naive way of measuring XY phase via the ODC would be to calculate the cross correlation $\mathbf{w}_y^H \mathbf{R} \mathbf{w}_x$ between X and Y PAF beams on the same ASKAP dish. Here $\mathbf{R} = \left\langle \mathbf{v}_{\text{paf}} \mathbf{v}_{\text{paf}}^H \right\rangle$ is the time-averaged 188×188 covariance matrix of PAF voltages. Normally, when dominated by receiver

noise and not observing a polarised source, the correlation between X and Y beams would be small because we know there is little natural leakage between X and Y PAF beams (Sault, 2014). However, we expect an easily measurable XY correlation when the PAF is illuminated by the linearly polarised ODC source that is oriented at 45° to the primary polarisation planes of the PAF elements. Further, assuming that the instrumental polarisation leakage is small as shown by Sault (2014), we expect the phase of this XY correlation to be approximately the XY phase of that dual-polarisation pair of beams.

However, if the ODC signal is on during beam weight calculation, the maxSNR weights will naturally suppress the ODC signal (Chippendale et al., 2018). This is good for minimising noise in astronomical observations, but unhelpful for estimating XY phase because we have essentially cancelled the calibration signal. A conservative solution might be to turn the ODC signal off during beamforming, on for XY phase calibration, and then off again during astronomical measurements. However, we sought a solution to the cancellation problem that would allow the ODC signal to be left on at all times. Our solution enables a more versatile system where changes in port gains and beam polarisation can be continuously estimated and calibrated during scientific observations.

First, we define the reference port for the weights of each polarisation to be the port corresponding to largest amplitude in $\mathbf{w}'_x$ and $\mathbf{w}'_y$ respectively

$$i_{\text{max}} = \arg\max_i |w'_i|. \tag{5.3}$$

Instead of letting this reference port change between each 1 MHz beamformer channel, we select the largest amplitude element in the median sense across all frequency channels. As demonstrated by Chippendale et al. (2016), we expect the form of $\mathbf{w}'$ to be close to the Airy diffraction pattern associated with the finite aperture of the paraboloidal reflector. This will have a main lobe of a certain phase then sidelobes that alternate in phase by 180° with respect to the main lobe.

Second, we identify all ports that satisfy

$$\left|\text{Arg}(w'_i / w'_{i_{\text{max}}})\right| < \pi/4. \tag{5.4}$$

This selects ports in the main lobe and even numbered sidelobes. We then estimate XY phase as

$$\phi_{xy} = \text{Arg}\left(\sum_{i\in\Omega_y} w'_{y,i} \Big/ \sum_{i\in\Omega_x} w'_{x,i} \right). \tag{5.5}$$

The sums in the numerator and denominator are taken over the the set of elements Ω defined by selecting the 16 elements of largest amplitude from the set of elements that satisfy (5.4). These vector sums bias phase estimates towards their values in the main lobe of the Airy pattern. Limiting the sum to the 16 strongest elements helps reject the second sidelobe which is the same phase as the main lobe and does fall on the PAF for edge beams at high frequencies.

Figure 5.1 compares the raw weights with those calibrated via the ODC signal. It is clear that the calibration makes the phase of the weights coherent within each lobe of the Airy diffraction pattern and yields the expected phase difference of 180° between the main lobe and the first sidelobe. The calibration has a less significant impact on weight amplitude because we have already normalised the gain of all PAF ports by adjusting their RF attenuators. There is however

one port in the first sidelobe that has an overly strong weight amplitude, but after calibration has a weight that is comparable to other ports in the same sidelobe.

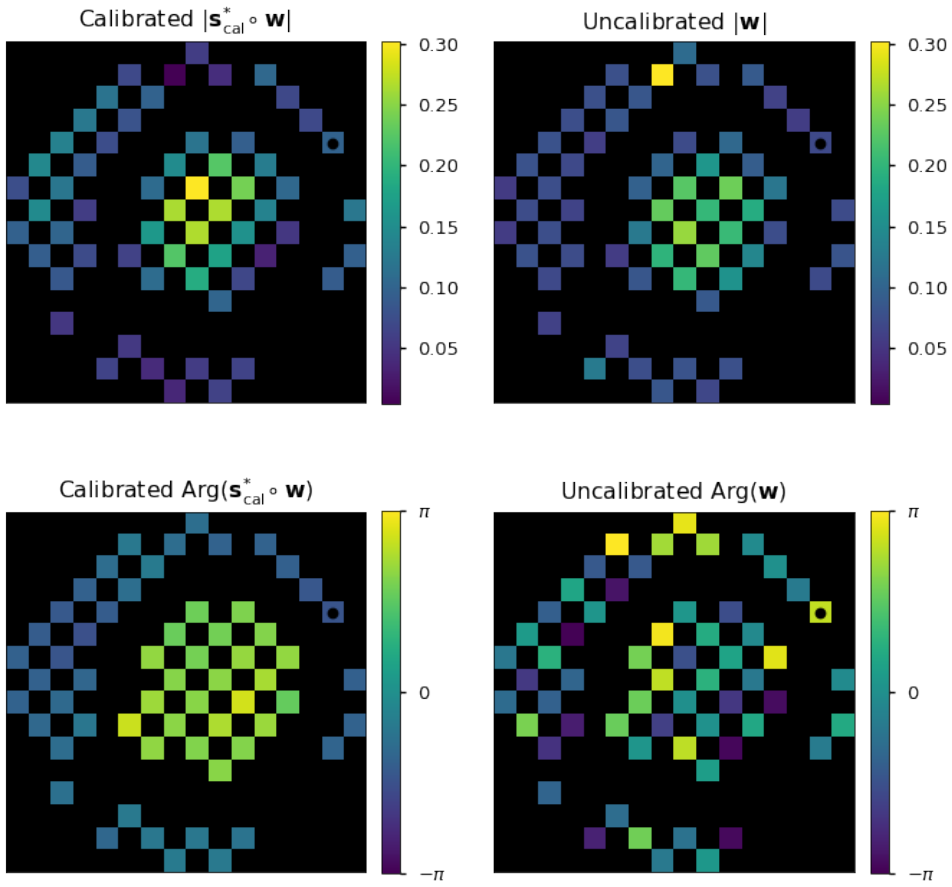

Figure 5.1: Comparison of calibrated (left) and uncalibrated (right) weights for beam 2 (counting from 0) of ak14 at 715 MHz. Ports not included in the weights at all are coloured black. PAF port one is marked by a black circle.

We filter the XY phase estimates over frequency to smooth out narrow-band corruption due to RFI and narrow-band measurement errors. The general approach is to smooth a noisy phase measurement that has some invalid (NaN) data, some narrow-band outliers (RFI), and a dominant linear phase (delay) component. The algorithm used is as follows:

1. Estimate the linear phase gradient via Fourier transform.
2. Remove the linear phase gradient (multiply by conjugate phasor).
3. Fit a low-order polynomial to valid data points (excluding nan values and outliers).
4. Replace the invalid (NaN) data and outliers (RFI) with the evaluated polynomial.
5. Apply a median filter.
6. Restore the linear phase gradient (multiply by phasor).

Both beamformer weights and XY phase estimates are calculated independently for each 1 MHz channel. In the future we should explore jointly solving for weights across all frequencies with a smoothness constraint (e.g. gradient regularization Giraud et al., 2019) or interpolating weights at RFI affected frequencies (Chippendale and Hellbourg, 2017) before applying the XY phase

calibration discussed here. Either of these options may avoid the need to smooth XY phase estimates as described above.

Once XY phase is estimated we multiply the Y polarisation beamformer weights by a complex phasor of amplitude unity and with phase equal to the XY phase estimate

$$\hat{\mathbf{w}}_y = e^{j\phi_{xy}} \mathbf{w}_y. \tag{5.6}$$

6 Validation of New Technique

6.1 Validation of XY Phase Estimation via ODC

We validated XY phase estimation via ODC by performing a rotated-antenna XY phase measurement with the ODC noise sources on during beamforming and polarisation calibration. For this experiment antenna ak01 was rotated by +5° about it's roll axis and ak02 was rotated by -5° during both the beamforming observation and the observation for calibrating polarisation and bandpass. A `square_6x6` beam footprint on 0.9° pitch with 45° footprint rotation and a centre frequency[1] of 864.5 MHz was calibrated on the Sun using the usual technique in scheduling block `SB5030` resulting in the weights set `SB05030_201801250718_FILT_1200_36beam`. These weights were then applied to ASKAP's beamformers and used to make a polarisation and bandpass calibration observation in `SB5031`. The telescope was steered to sequentially put PKS B1934−638 in each of the 36 beams for a 200 second integration in each.

The dedicated polarisation pipeline was applied offline to estimate XY phase from the rotated-antenna bandpass measurement in `SB05031`. Independently, the new technique for estimating XY phase, via the radiated ODC signal, was applied to the PAF covariance matrices collected during the beamforming measurement in `SB5030` and the exact beamformer weights that were derived from them and applied in the rotated-antenna calibration measurement. Figure 6.1 compares the resulting XY phase estimates from both techniques for ASKAP antenna ak05. The agreement between both techniques is good except for beam 35 (counting from zero). We suspect an out-by-one indexing error caused this final beam not to be correctly processed for the rotated-antenna data.

We had to add 180° to all XY phase estimates from the ODC technique to make them agree with the rotated-antenna technique. A sign error has also been observed in rotation measures calculated from ASKAP data. We are currently reviewing coordinate definitions for the antenna and PAF (Reynolds, 2014) and the Stokes definitions used in ASKAP software to better understand the full polarisation definitions of the ASKAP array and software as built.

The comparison measurements discussed here were made with 16 ASKAP antennas, of which 12 had working ODC systems. Additionally, ak03 and ak06 suffered beamformer errors during the measurements and so were excluded from analysis. We were therefore able to make a quantitative comparison between the two techniques over 240 MHz in 36 beams on 10 antennas. After inspection of the data, we decided to exclude outliers from the quantitative analysis including beam 11 on ak17, beam 15 on ak24, beam 20 on ak10 and beams 30, 32 and 35 on all

[1] The hardware was configured with a requested centre frequency (CF) of 864 MHz, the CF in the parset was 864.5 MHz which is also the centre frequency of the 336 MHz bandwidth available at the beamformer and recorded in weights and ACM files. At the time, the correlator had a reduced bandwidth of 240 MHz which was centred on 913.5 MHz

antennas. We take the difference of the XY phase between the two techniques to be an estimate of the XY-phase error (although we don't know which technique is the more accurate one).

Since the results from the two techniques obviously track each other closely, the band-average and band-median XY phase difference provide an effective estimates of how much power will leak from linear to circular polarisation in a typical multi-frequency synthesis imaging analysis. In addition, where appropriate, we provide percentiles for the frequency-dependent deviation between the techniques over the band. This is relevant for determining how much power in a circular polarisation spectrum may be a spurious and frequency-dependant response to linear polarisation.

The median band-average XY-phase error per beam over all antennas and beams (excluding outliers) was 0.34° and the interval containing and the 2.5th and 97.5th percentiles (i.e. interval containing 95% of the band-average error estimates) is [-4.4°, 5.0°].

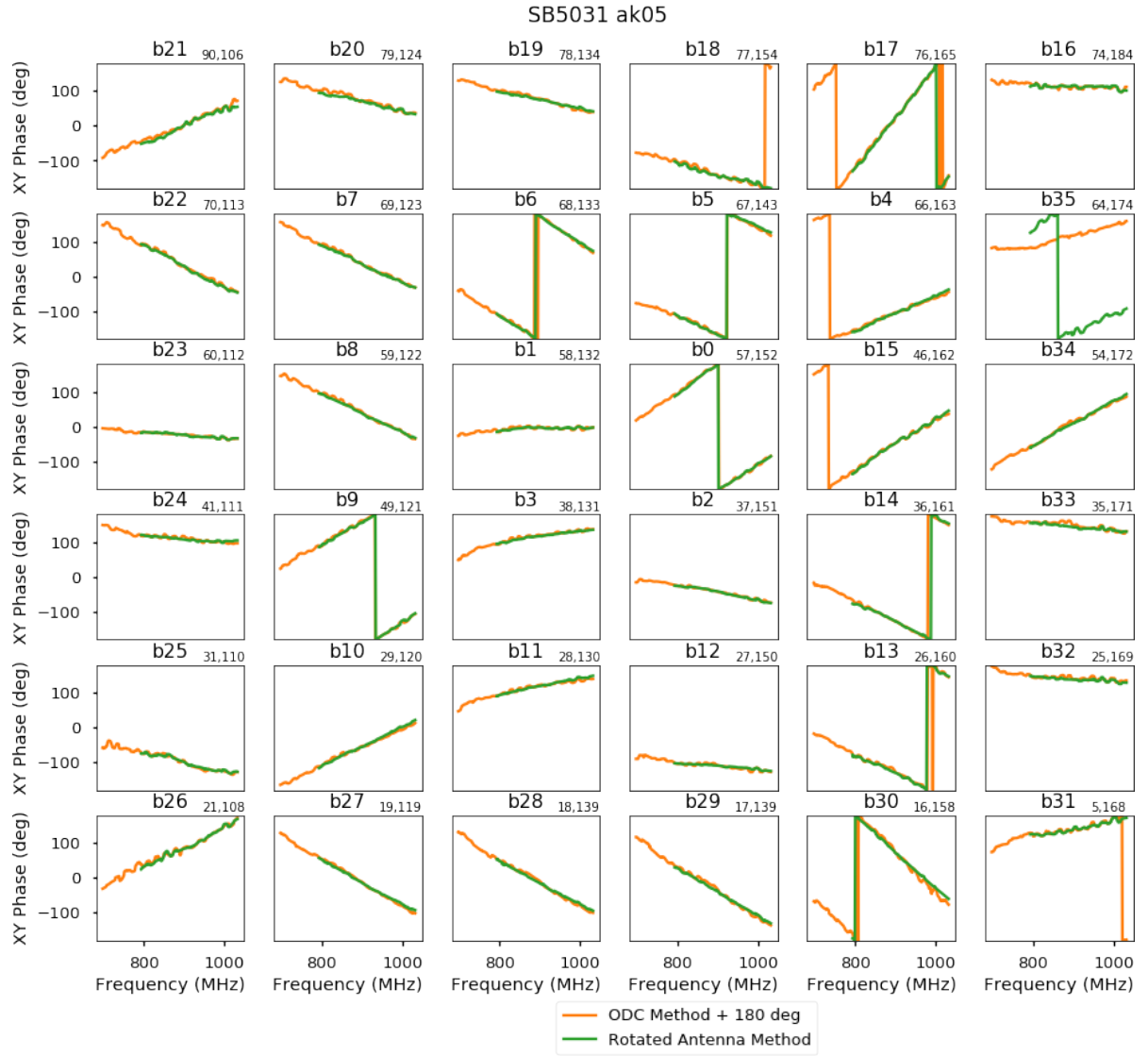

Figure 6.1: Comparison of XY phase estimates between new ODC technique and old rotated antenna technique.

Figure 6.2 shows the overall distribution of band-average difference (error) between the old and new XY phase estimates over all beams and antennas, including the impact of removing the outlier antennas/beams from the analysis as discussed above. Figure 6.3 uses box plots to segment and compare the error distribution between antennas. Figures 6.4 and 6.5 show summaries of the standard deviation and mean of XY phase errors for each beam on every antenna. For each antenna, the pixels in the plot are arranged according to the "footprint" of the beams on the sky.

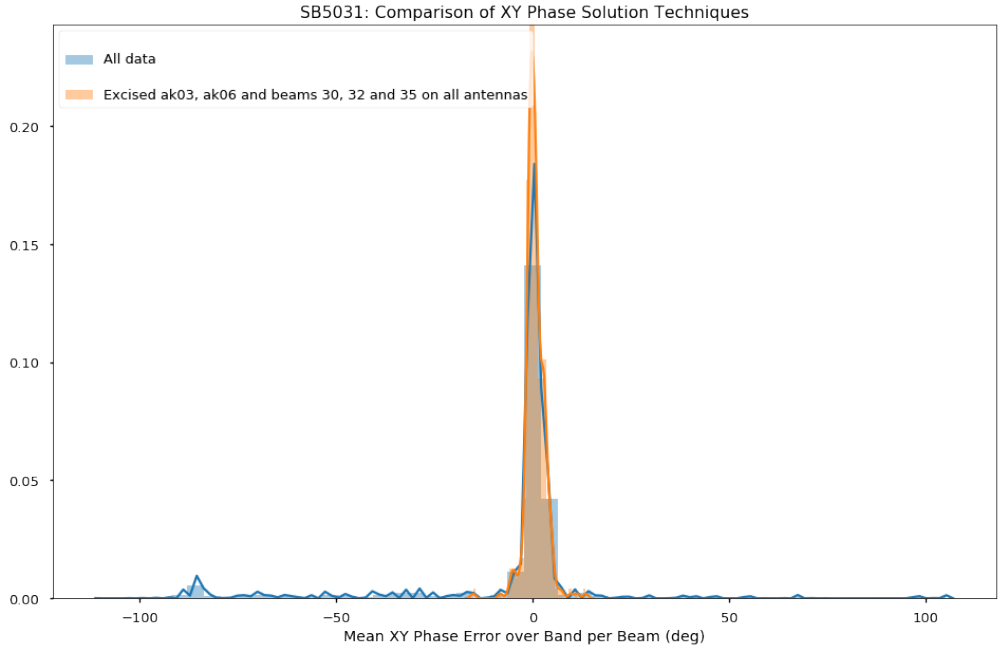

Figure 6.2: Overall distribution of band-average difference (error) between old and new XY phase estimates over each beam and antenna.

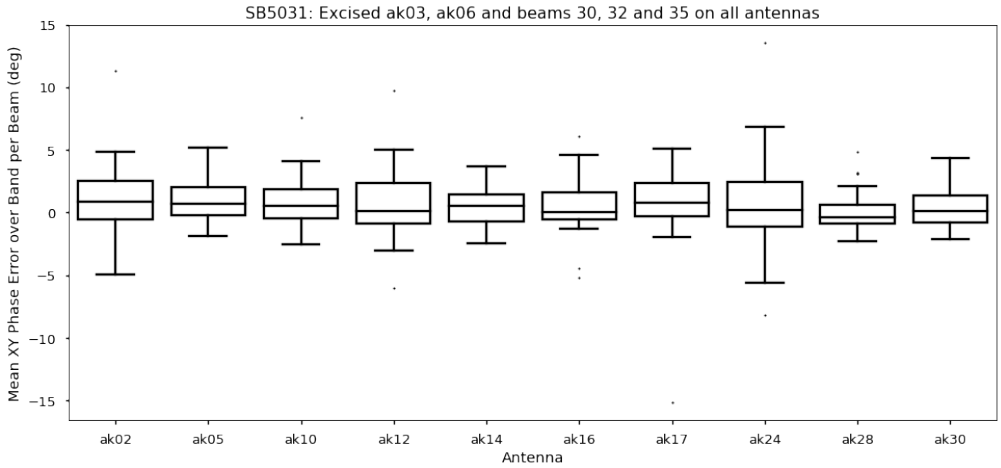

Figure 6.3: Distributions of band-average difference (error) between old and new XY phase estimates over 36 beams for each antenna.

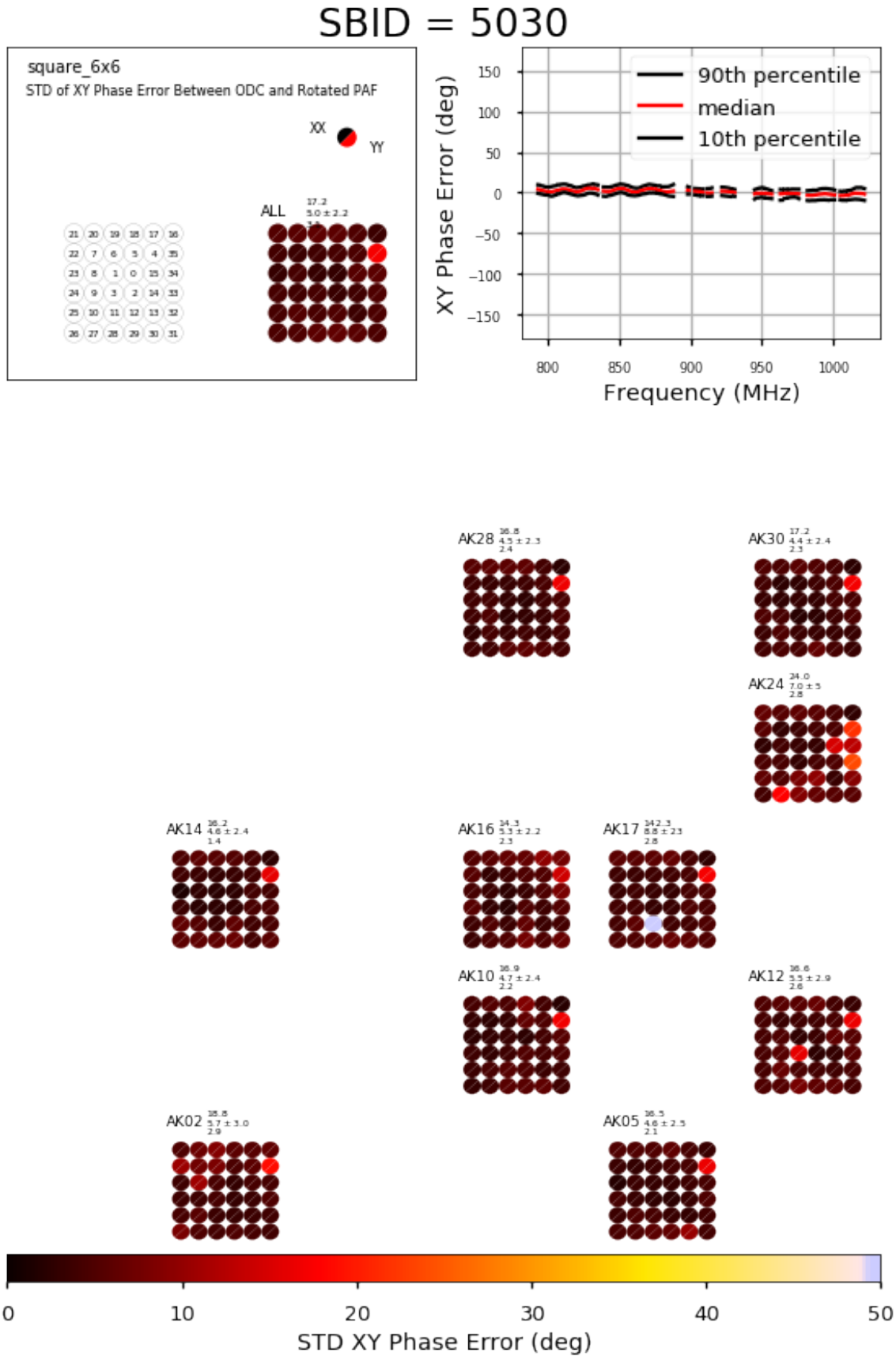

Figure 6.4: Summary of the standard deviation of error between ODC and rotated antenna estimates of XY phase over 36 beams on 10 antennas.

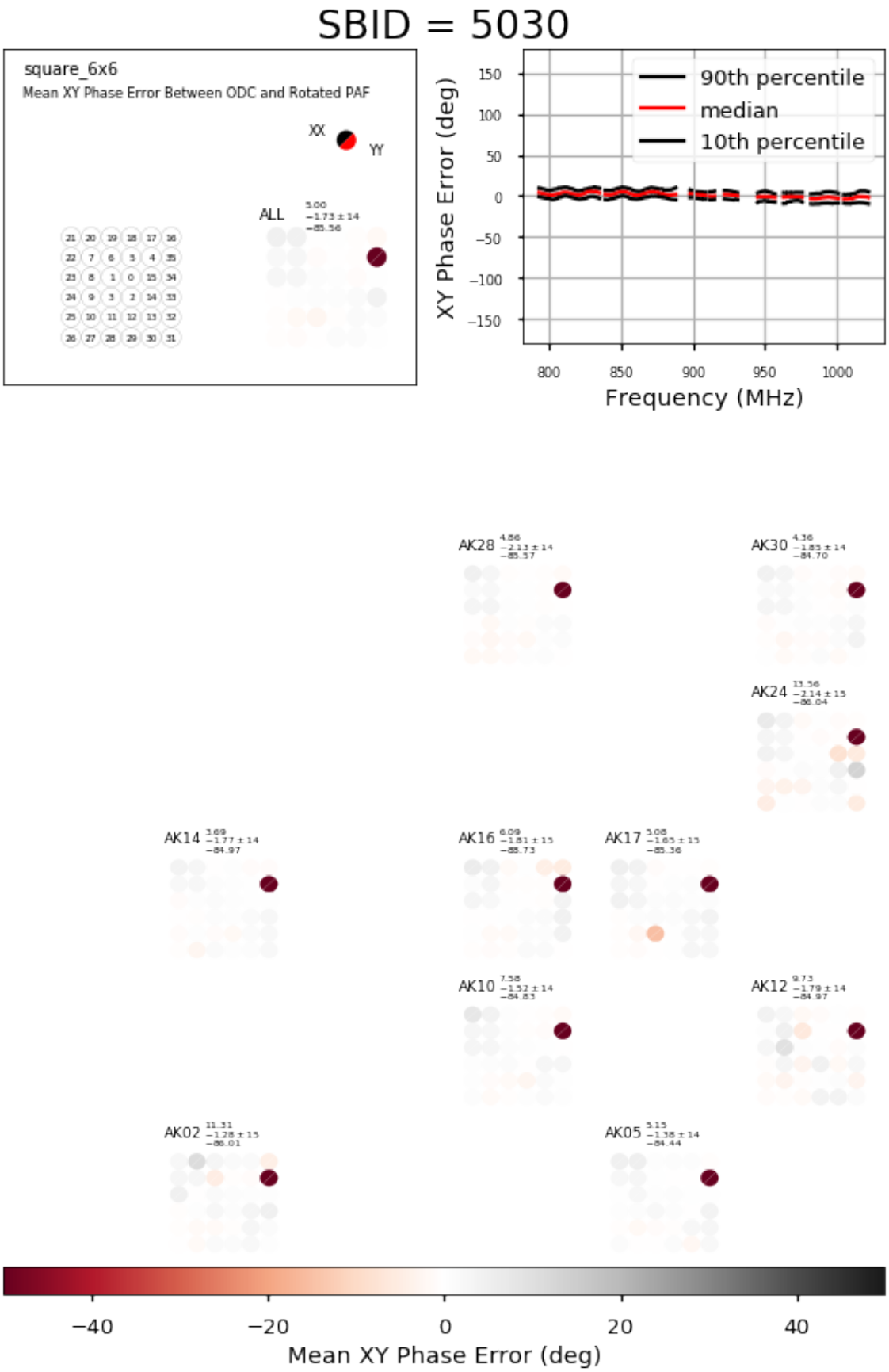

Figure 6.5: Summary of the mean error between ODC and rotated antenna estimates of XY phase over 36 beams on 10 antennas.

6.2 Validation of XY Phase Correction in Beamformer Weights

The next step was to make a second rotated-antenna measurement of XY phase, but with weights loaded in the beamformers that had already had XY phase estimated and corrected via the new ODC technique. The desired result of this experiment is to measure near-zero XY phase for all antennas that have working ODC systems.

The first experiment used a single beam only: The calibrator PKS B1934-638 was observed with ASKAP-28 in beam 0 for a routine bandpass calibration. Antennas ak01 and ak02 had their PAFs rotated by 5 degrees in opposite directions. The rotated PAF method was used to calculate the on-axis polarisation leakages in each 1 MHz channel across the 288 MHz band. If the zero XY phase condition is met, we expect the leakage from the X beam on the antennas with the rotated PAFs into the Y beam on all other antennas, and similarly for the Y-into-X beam leakage, to be purely real-valued signal with an amplitude of $\sin(5^\circ) \approx 0.09$. Figure 6.6 broadly shows that this is the case, largely verifying the ability of the new beam-forming technique to null the XY phase over the full band.

Second-order imperfections remain: The real part of the leakage continues to dominate, suggesting that minor rotational misalignments exist between PAFs between antennas. This can be corrected to first order with a frequency-independent leakage calibration or by measuring the roll-axis offsets and compensating for them in the antenna pointing models. However, small-period coherent oscillatory structure is also apparent in both the real and imaginary parts of the leakage. The cause of this will be investigated, but may be due to standing waves caused by reflections of the ODC signal between the PAF and reflector surface. This could in principle be corrected with a frequency-dependent leakage calibration, but might also be corrected at the beam-forming stage with refinements to the ODC signal processing.

We did not add the unexplained 180° to the XY phase estimate used to correct beamformer weights in this final validation, despite it being required in section 6.1 for the rotated-antenna and ODC methods to agree. We left the sign as is required to align the phase of X and Y polarisation signals in actual measurements. It is clear from bandpass observations and online visualisation of phases on individual baselines that X and Y beams are very close to one another in phase when XY phase is corrected in the beamformer weights. We are thus applying the correction as required in hardware as built, but must do more work to fully understand polarisation and Stokes definitions of the end-to-end ASKAP system including software. Current work towards understanding ASKAP's polarisation definitions includes assessing the polarimetric response of ASKAP to a strongly polarised source with measurable circular polarisation of known hand (Vela) and the checking of the sign of Faraday rotation measures of radio sources derived from ASKAP data against results from other telescopes.

7 Discussion

We note the following insights, opportunities, and residual issues precipitated by the current work:

Insights

- The bulk of XY phase appears to be a linear phase slope with frequency suggesting the dominant effect we are calibrating is a delay between X and Y beams, likely due to differing cable lengths between the dominant contributing PAF port in each of the X and Y beams.

- Having X and Y beams aligned in phase also makes online visualisation of visibilities simpler and more intuitive

Opportunities

- This technique could be extended to correct relative delays between beams on each antenna.

Residual Issues

- Further work is required to understand the feed coordinates and polarisation (Stokes) definitions for the end-to-end ASKAP system including software.
- The 180° discrepancy between the rotated-antenna and ODC methods of estimating XY phase must be resolved.
- We need to understand and attempt to mitigate the frequency-dependent structure in the XY phase residuals after the bulk of XY phase is corrected via the ODC.
- We should exclude ports from beamforming that have abnormally low responses to the ODC signal.
- If an ODC fails, then the XY phase correction is not applied to the beam weights on the associated antenna. This needs to be recorded in the observation variables in the scheduling block database so post-processing can act accordingly.
- A large phase step can occasionally occur halfway through the band on one antenna with XY-phase-corrected beam weights. See `SB07745`.
- We should select the 60 ports weighted into each beam based on their contribution to beamformed SNR instead of by weight amplitude.

8 Conclusion

We have successfully estimated the XY-phase of PAF beams via an external noise source source and demonstrated adjustment of beamformer weights so that the XY phase of each dual-polarisation beam pair is near zero by design. Our new technique yielded a band-average XY phase of $0.34^{+5}_{-4.4}$ degrees for 95% of PAF beams when compared to the rotated-antenna method of XY phase calibration. Calibrating XY phase up-front in the beamformer weights allows polarisation calibration and imaging to take place within the standard ASKAP software pipeline. This allows polarisaiton studies to be made commensaly with all ASKAP observations.

Acknowledgements

Thanks to Aidan Hotan for executing the test observations on ASKAP that we analysed here.

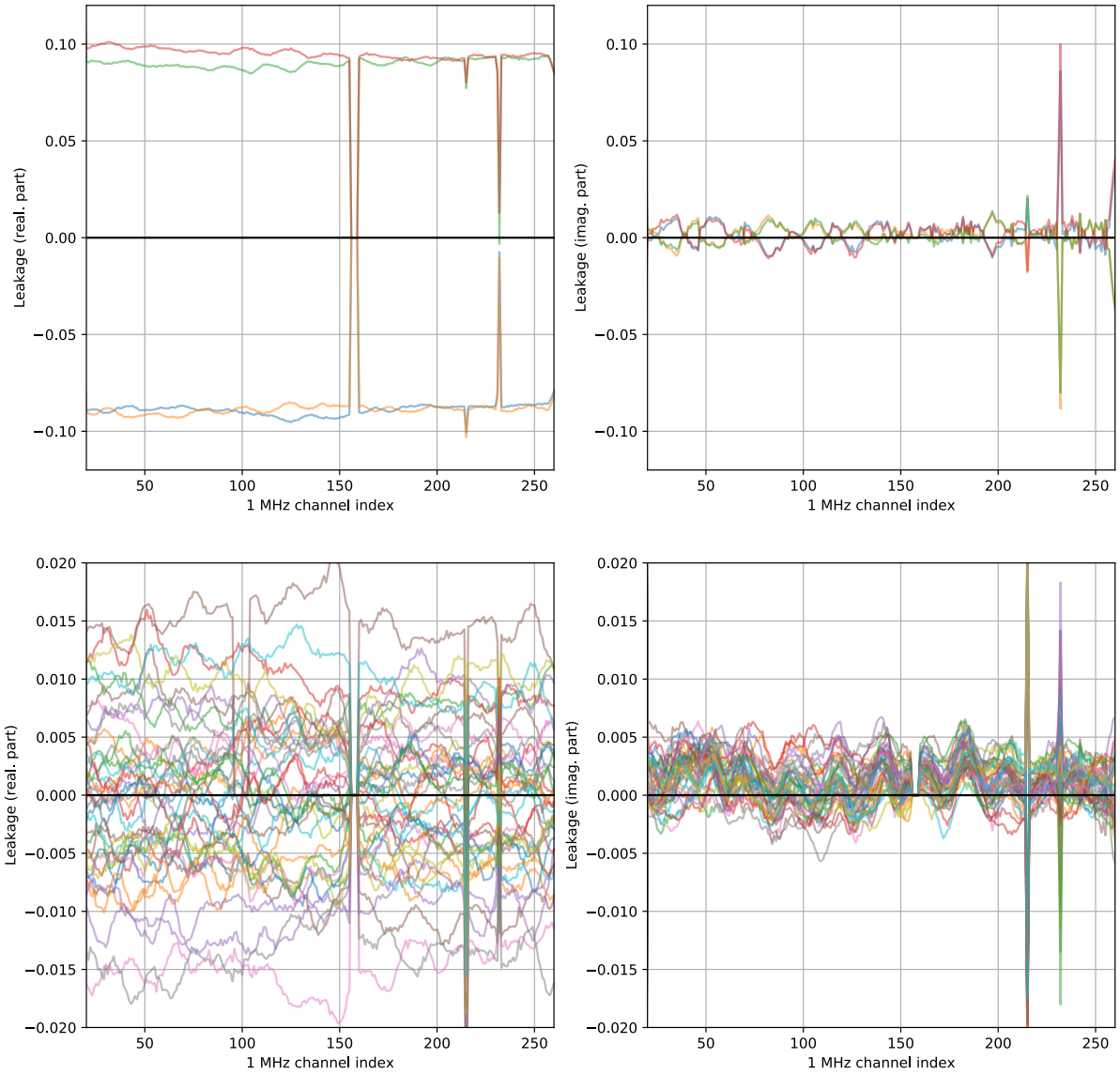

Figure 6.6: Top: Real (left) and imaginary (right) parts of the leakage for antennas ak01 and ak02, which had PAFs rotated by 5 degrees in opposite directions, calculated on a per-MHz-channel basis from observations of the calibrator PKS B1934-638 by assuming that it is unpolarised (accurate to 0.1%). The expectation for zero XY phase is a purely real-valued signal with an amplitude of $\sin(5^\circ) \approx 0.09$. the large spikes near channels 155, 220, and 280 are due to RFI-afflicted measurements. Bottom: The same, but calculated for antennas with no intentional PAF rotation. Note the different y-axis scale to the top panels.

References

Craig Anderson, George Heald, Shane O'Sullivan, John Bunton, Ettore Carretti, Aaron Chippendale, Jordan Collier, Jamie Farnes, Bryan Gaensler, Lisa Harvey-Smith, Bärbel Koribalski, Tom Landecker, Emil Lenc, Naomi McClure-Griffiths, Daniel Mitchell, Lawrence Rudnick, and Jennifer West. The Extraordinary Linear Polarisation Structure of the Southern Centaurus A Lobe Revealed by ASKAP. *Galaxies*, 6:127, Nov 2018. doi: 10.3390/galaxies6040127.

R. Beresford, M Leach, A. P. Chippendale, and D. Hayman. ASKAP on-dish calibration system. In *Phased Array Feed Workshop*, September 2018.

A. J. Brown, G. A. Hampson, P. Roberts, R. Beresford, J. D. Bunton, W. Cheng, R. Chekkala, D. Kiraly, S. Neuhold, and K. Jeganathan. Design and implementation of the 2nd generation ASKAP digital receiver system. In *2014 International Conference on Electromagnetics in Advanced Applications (ICEAA)*, pages 268–271, August 2014. doi: 10.1109/ICEAA.2014.6903860.

A. P. Chippendale and G. Hellbourg. Interference mitigation with a modified ASKAP phased array feed on the 64 m Parkes radio telescope. In *2017 International Conference on Electromagnetics in Advanced Applications (ICEAA)*, pages 948–951, Sep. 2017. doi: 10.1109/ICEAA.2017.8065413.

A. P. Chippendale, D. McConnell, K. Bannister, N. Nikolic, A. W. Hotan, K. W. Smart, R. D. Shaw, D. B. Hayman, and S. G. Hay. Recent developments in measuring signal and noise in phased array feeds at CSIRO. In *2016 10th European Conference on Antennas and Propagation (EuCAP)*, pages 1–5, April 2016. doi: 10.1109/EuCAP.2016.7481741.

A. P. Chippendale, C. Button, and L. Lourenco. Measuring ASKAP's on-dish calibration signal level and its impact on beam sensitivity. ACES Memo 1, CSIRO, June 2018. URL http://www.atnf.csiro.au/projects/askap/ACES-memos.

J. Dowson. The utility of the ASKAP on-dish calibration system. ACES Memo 17, CSIRO, July 2017. URL http://www.atnf.csiro.au/projects/askap/ACES-memos.

J. Giraud, M. Lindsay, V. Ogarko, M. Jessell, R. Martin, and E. Pakyuz-Charrier. Integration of geoscientific uncertainty into geophysical inversion by means of local gradient regularization. *Solid Earth*, 10(1):193–210, 2019. doi: 10.5194/se-10-193-2019. URL https://www.solid-earth.net/10/193/2019/.

G. A. Hampson, A. Brown, J. D. Bunton, S. Neuhold, R. Chekkala, T. Bateman, and J. Tuthill. ASKAP Redback-3 an agile digital signal processing platform. In *2014 XXXIth URSI General Assembly and Scientific Symposium (URSI GASS)*, pages 1–4, August 2014. doi: 10.1109/URSIGASS.2014.6930062.

D. McConnell et al. The Australian Square Kilometre Array Pathfinder: Performance of the Boolardy Engineering Test Array. *Proc. Astron. Soc. Aust.*, 33:e042, September 2016. doi: 10.1017/pasa.2016.37.

J. E. Reynolds. Beam geometry in ASKAP. ACES Memo 18, CSIRO, October 2014. URL http://www.atnf.csiro.au/projects/askap/ACES-memos.

R. J. Sault. Initial characterisation of BETA polarimetric response. ACES Memo 2, CSIRO, September 2014. URL http://www.atnf.csiro.au/projects/askap/ACES-memos.

K. W. Weiler. The Synthesis Radio Telescope at Westerbork. Methods of Polarization Measurement. $A\&A$, 26:403, August 1973.

CONTACT US

t 1300 363 400
+61 3 9545 2176
e csiroenquiries@csiro.au
w www.csiro.au

WE DO THE EXTRAORDINARY EVERY DAY

We innovate for tomorrow and help improve today for our customers, all Australians and the world.

Our innovations contribute billions of dollars to the Australian economy every year. As the largest patent holder in the nation, our vast wealth of intellectual property has led to more than 150 spin-off companies.

With more than 5,000 experts and a burning desire to get things done, we are Australias catalyst for innovation.

WE IMAGINE. WE COLLABORATE. WE INNOVATE.

FOR FURTHER INFORMATION

Astronomy and Space Science
Dr. Aaron Chippendale
t +61 2 9372 4296
e Aaron.Chippendale@csiro.au
w www.atnf.csiro.au